LANGMUIR Article
Cite This: Langmuir 2018, 34, 572–584
pubs.acs.org/Langmuir

Instability Mechanisms of Water-in-Oil Nanoemulsions with Phospholipids: Temporal and Morphological Structures

Jan-Hendrik Sommerling,[†,‡] Maria B. C. de Matos,[‡,§] Ellen Hildebrandt,[†,‡] Alberto Dessy,[‡] Robbert Jan Kok,[§] Hermann Nirschl,[†] and Gero Leneweit*[,‡,∥]

[†]Institute for Mechanical Engineering and Mechanics, Karlsruhe Institute of Technology, Straße am Forum 8, 76131 Karlsruhe, Germany

[‡]Abnoba GmbH, Hohenzollernstraße 16, 75177 Pforzheim, Germany

[§]Utrecht Institute for Pharmaceutical Sciences, Department of Pharmaceutics, Utrecht University, 3512 JE Utrecht, The Netherlands

[∥]Carl Gustav Carus-Institute, Association for the Advancement of Cancer Therapy, Am Eichhof 30, 75223 Niefern-Öschelbronn, Germany

Supporting Information

ABSTRACT: Many food preparations, pharmaceuticals, and cosmetics use water-in-oil (W/O) emulsions stabilized by phospholipids. Moreover, recent technological developments try to produce liposomes or lipid coated capsules from W/O emulsions, but are faced with colloidal instabilities. To explore these instability mechanisms, emulsification by sonication was applied in three cycles, and the sample stability was studied for 3 h after each cycle. Clearly identifiable temporal structures of instability provide evidence about the emulsion morphology: an initial regime of about 10 min is shown to be governed by coalescence after which Ostwald ripening dominates. Transport via molecular diffusion in Ostwald ripening is commonly based on the mutual solubility of the two phases and is therefore prohibited in emulsions composed of immiscible phases. However, in the case of water in oil emulsified by phospholipids, these form water-loaded reverse micelles in oil, which enable Ostwald ripening despite the low solubility of water in oil, as is shown for squalene. As is proved for the phospholipid dipalmitoylphosphatidylcholine (DPPC), concentrations below the critical aggregation concentration (CAC) form monolayers at the interfaces and smaller droplet sizes. In contrast, phospholipid concentrations above the CAC create complex multilayers at the interface with larger droplet sizes. The key factors for stable W/O emulsions in classical or innovative applications are first, the minimization of the phospholipids' capacity to form reversed micelles, and second, the adaption of the initial phospholipid concentration to the water content to enable an optimized coverage of phospholipids at the interfaces for the intended drop size.

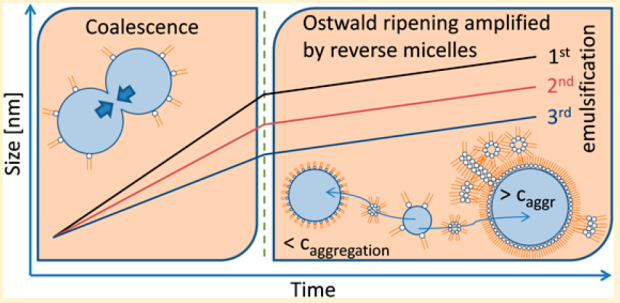

INTRODUCTION

Water-in-oil (W/O) emulsions are regularly used in many food preparations, pharmaceutics, and cosmetics. Commonly, these dispersed systems are stabilized by increasing the viscosity of the continuous phase and thus nearly immobilizing droplets. Phospholipids (PLs) are widely used emulsifiers as they are gained from natural, sustainable sources[1] with approved biocompatibility regarded as a substance that is "generally recognized as safe" (GRAS) by the Food and Drug Administration (FDA)[2] due to their ubiquitous occurrence in humans as in most organisms. PLs are commonly used as emulsifiers for oil-in-water (O/W) emulsions but are faced with unexplored instability problems in W/O emulsions. This contradicts the expectations raised by their hydrophilic–lipophilic balance (HLB) value, which for dipalmitoylphosphatidylcholine (DPPC) is around 5, which indicates their suitability as an W/O emulsifier.[3] Further arguments to explore their use in W/O emulsification are the high solubility of phospholipids in most oil phases and their molecular shape. The molecular geometry is comparable to a cylinder or cone, depending on the degree of saturation of the fatty acids and the size of the hydrophilic group. It makes them more suitable for W/O than for O/W emulsions when considering interfacial curvatures—a contradiction that has not yet been solved rigorously in the literature.[4] W/O emulsions consisting of two low-viscous phases emulsified by phospholipids are frequently reported as unstable.[1,5] However, more stable W/O emulsions based on PL could trigger new applications in a wide range of pharmaceutical and food-related products and lead to innovations.

The stability of an emulsion is governed by the emulsifier at the interface between continuous and dispersed phase, as well

Received: August 12, 2017
Revised: October 22, 2017
Published: December 8, 2017

DOI: 10.1021/acs.langmuir.7b02852
Langmuir 2018, 34, 572–584

as the viscosity of the continuous phase and density difference of the two immiscible phases.[6] During emulsification, the diffusion speed of the surfactant is crucial to the initial coverage of the interface and therefore for the size distribution and stability of the emulsion.[7] PLs have a molecular weight of 700 to 800 g/mol and are therefore much slower in diffusion than other common surfactants like, e.g., SDS with a molecular weight of 288 g/mol. The duration and efficiency of the dispersion process are decisive for the choice of surfactant and vice versa. Mechanical dispersion methods differ significantly in input energy density, depending on the physical principle and residence time. High-shear mixers have a relatively low energy input, while high pressure homogenization and ultrasonication provide a higher energy input, which makes them especially suitable for fast diffusing surfactants.[8] During ultrasonication the sample is continuously mixed in a batch or pumped through a chamber,[9,10] while for high pressure homogenization the number of passages determines the residence time in combination with the mass flow. The optimal processing parameters for a homogenizer are in the high pressure range above 1000 bar with very fast mass flows and therefore short residence times $\ll$1 s,[11,12] which even for many passages does not lead to high residence times. For the relatively slow PLs, a dispersion process with the ability to form small droplets and long residence times is needed. Since high pressure homogenization can produce very small droplets, the method is not suitable for slow surfactants. High shear mixers cannot produce the desired size distribution below 1 μm. Ultrasonication was therefore the method of choice, allowing sufficiently long residence times and high shear forces with short intervals of energy input.

The adsorption kinetics of a surfactant in a liquid−liquid two phase system can be characterized with profile analysis tensiometry (PAT).[13−15] This time-dependent measurement of the dynamic interfacial tension also reveals the critical aggregation concentration (CAC) of a PL in an oil phase and the minimal area per molecule of the surfactant at the interface.

DPPC-based water in squalene nanoemulsions are used here as representative system for pharmaceutical emulsions.[16] Squalene is used as adjuvant in vaccines for its enhancing therapeutic effect and is becoming more important for emulsion systems as well.[17] Apart from the use of water/squalene systems in pharmaceutics and cosmetics, W/O emulsions are increasingly studied as precursors to produce liposomes.[18,19] W/O emulsions using PLs experience increasing interest in digital microfluidics[20] to mimic organismic conditions.

Previous findings show that DPPC and POPC, which are both regularly used as models for membrane PL, show very divergent CAC and interfacial packing density, due to the saturated and unsaturated groups, respectively, that interact differently with organic solvents. The minimum interfacial tensions in equilibrium are similar, suggesting that both could be suited for the use in nanoemulsions, but the morphological formation and differences in solubility can have an impact on the instability mechanism. In numbers, the CAC for DPPC is at 0.103 mM, while POPC has a 12-fold higher CAC of 1.256 mM, meaning the molecular solubility is higher. The packing density of the lipids at the oil−water interface also differs with 44 Å^2 per molecule for DPPC and 119 Å^2 per molecule for POPC with possible multilamellar structures occurring with DPPC.[21,22]

The aim of this study is to unravel the instability mechanisms of W/O emulsions with PL to find physical explanations for the short lifetime of such systems. Based on their understanding, innovative formulations can be developed, which consider adequate material properties, suitable relative quantities, and mechanical processing. This is necessary in order to produce stable W/O emulsions of the desired size with narrow droplet-size distributions suitable for topical or parenteral use as needed in most applications.[23]

EXPERIMENTAL SECTION

Materials. Squalene ($C_{30}H_{50}$) with 98% purity, was used as continuous phase for the emulsions, purchased from Sigma-Aldrich (Taufkirchen, Germany). Water for injection was used for the dispersed aqueous phase. Two different phospholipids were tested as emulsifiers, dipalmitoylphosphatidylcholine (DPPC) with saturated fatty acids (16:0, 16:0) and palmitoyloleoylphoshatidylcholine (POPC) with one saturated and one unsaturated fatty acid (16:0, 18:1). The purity of both phospholipids was >99%, kindly donated by Lipoid GmbH (Ludwigshafen, Germany). Emulsification was done mechanically with an ultrasound sonotrode, UP 200S with 200W maximum output, and an ultrasound frequency of 26 kHz from Hielscher Ultrasonics GmbH (Teltow, Germany). Photon correlation spectroscopy (PCS) measurements were performed using a Malvern Instruments (Worcestershire, UK) Zetasizer ZS90 with a wavelength of 633 nm at 90°: Profile analysis tensiometry was done using a PAT-1 device from Sinterface Technologies (Berlin, Germany).

Methods. The kinetics of interfacial adsorption of PL is crucial for the process parameters of emulsification and can be investigated by using profile analysis tensiometry (PAT). It allows monitoring the time scale of the adsorption and stabilization of a pendant drop and determination of the critical aggregation concentration (CAC) of a PL in the oil phase. These findings were transferred to the testing of emulsions. In order to compensate the slow diffusion speed of the PL in ultrasonic emulsification, a repetitive, stepwise dispersion process was established, which allows the PL concentration on the pendant drop surface to approach equilibrium. This scheme enables assessment of the change in emulsion stability after each redispersion of the same emulsion. Further, the growth rate of emulsion droplets and change of drop size distributions in metastable emulsions are systematically investigated via photon correlation spectroscopy (PCS) to identify the mechanisms of instability over time.

The droplet size in an emulsion was monitored for 180 min immediately after emulsification, after which the procedure was repeated twice consecutively on the same sample. Initially DPPC was dispersed in squalene with an ultrasonication bath, attaining a concentration of 0.03 mg/mL = 0.0409 mmol/L or 0.3 mg/mL = 0.409 mmol/L, which will be referred to in the following as 0.04 mM and 0.4 mM, respectively. In a first step, emulsions were produced with 0.4 vol % water in the DPPC/squalene solution, premixing continuously for 10 s followed by sonication for 10 min with a sonication cycle of 0.5 s per second, both at an amplitude of 40% of the maximum output. The temperature was controlled with a −15 °C cooling rack, compensating for the heat input from sonication. In a second step, the emulsions were diluted to a final concentration 0.08 vol % water with squalene containing DPPC, keeping lipid concentration constant. The diluted emulsion was then sonicated once more for 5 min. The total process of (i) premixing, (ii) sonication for 10 min, (iii) dilution and (iv) sonication for 5 min is summarized as first sonication in the following. Emulsions were then measured with PCS for 180 min at 20 °C, recording size continuously. For the subsequent measurements, a second sonication of 10 and 180 min measurement were applied followed by a third sonication of 10 min and a final measurement of 250 min. Premixing and dilution was only applied for the first sonication, but not for the second and third, keeping concentrations constant for all three PCS measurements.

Results of the PCS measurements are provided in terms of z-average, polydispersity index (PDI), derived count rate (DCR) and

DOI: 10.1021/acs.langmuir.7b02852
Langmuir 2018, 34, 572−584

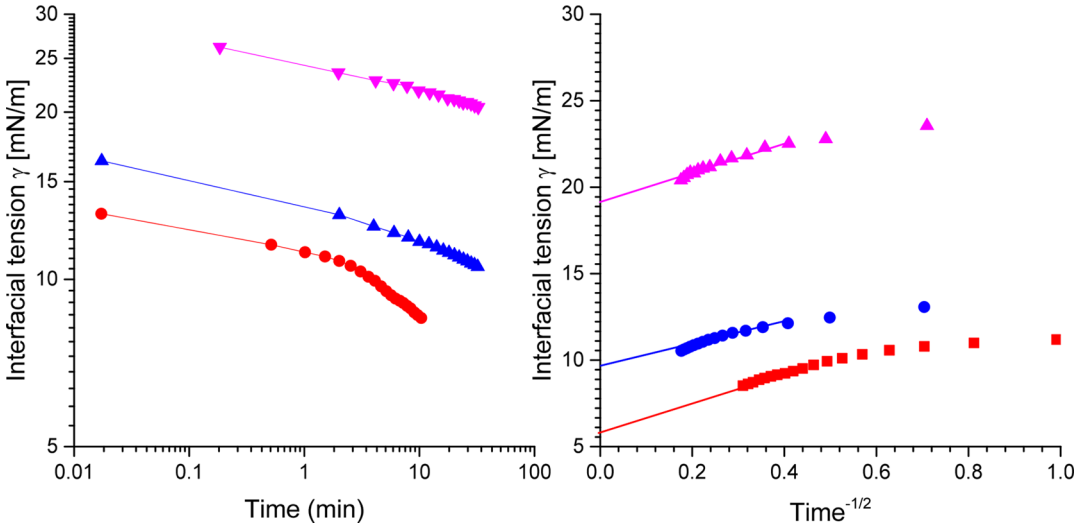

Figure 1. Adsorption kinetics of DPPC in squalene when exposed to a newly formed interface with water, measured by PAT tensiometry as described by Hildebrandt et al.[21] The interfacial tension γ decreases over time, as DPPC molecules adsorb at the interface for concentrations of ● 0.5 mM,▲ 0.05 mM, and▼ 0.01 mM. The left-hand side shows an biexponential plot to document the nonequilibrium state, while the right-hand side allows to extrapolate the equilibrium in the limit of $t(\infty)$, enabled by plotting γ versus $t^{-1/2}$.

intensity weighted size distributions. The z-average is calculated from the autocorrelation function by means of a third degree polynomial, as an intensity weighted monomodal mean size. The PDI is also gained from the autocorrelation and indicates the distribution by quantifying the divergence of the autocorrelation to a unimodal size signal. A high value in PDI indicates an insufficient fit of the model, therefore it is generally accepted that results above the threshold value of 0.7 cannot be described with the unimodal model. The count rate is a quantitative value for the light intensity on the photosensor and given in kilo counts per second, while the derived count rate includes signal attenuation during the measurement. Since Rayleigh scattering is the governing physical principle, the intensity is changed by particle size as well as sample concentration and cannot be attributed exclusively to a single effect. All size distributions were also evaluated by fitting the autocorrelation with a multiexponential function to account for multimodal distributions.

Tensiometry was performed with a series of defined DPPC concentrations in squalene over a time scale of 2000 s = 33 min, as described in more detail in Hildebrandt et al.[21,22] Images of the water drop in oil were taken and dynamical interfacial tensions were determined. Equilibrium interfacial tensions γ_e were acquired from a γ versus $1/\sqrt{t}$ diagram with an extrapolation for $t \rightarrow \infty$. The determination of the critical aggregation concentration (CAC) was acquired via the Gibbs adsorption isotherms, as described by Li et al.[15]

THEORETICAL BACKGROUND

The radius dependent solubility $S(r)$ of a substance dispersed in spherical droplets is given in relation to the solubility at a flat interface, i.e., sphere of infinite radius[24] $S(\infty)$:

$$S(r) = S(\infty)\exp\left(\frac{2\gamma V_m}{rRT}\right) \tag{1}$$

with γ being the interfacial tension between both phases, V_m the molar volume of the dispersed phase, R the gas constant and T the absolute temperature. The ratio of solubilities is referred to as the Ostwald equation. Lifshitz and Slyozo[25] derived a rate of droplet grow produced by Ostwald ripening:

$$\omega = \frac{\mathrm{d}}{\mathrm{d}t}(r_c^3) = \frac{8}{9}\frac{DS(\infty)V_m}{RT} \tag{2}$$

with r_c being the critical radius of a droplet neither growing nor decreasing, and D the diffusion coefficient of the disperse phase in the continuous phase. Ostwald ripening can be inhibited by means of adding ingredients that create higher osmotic pressure in the droplets, counteracting the migration of molecules.[26,27]

For droplets growing owing to coalescence, there is no well-accepted theoretical approach so far.[1] Deminiere et al.[28] assumed a growth mechanism based on the differential

$$\mathrm{d}N = -fA\mathrm{d}t \tag{3}$$

where $A = N\pi d^2$ is the total area of contacts, $N = 6V/(\pi d^3)$ is the number of droplets of a diameter d, formed by a fixed volume V of the disperse phase, and f is the frequency of coalescence. Deminiere et al.[28] found the evolution of the diameter based on the initial diameter to be

$$\frac{1}{d^2} = \frac{1}{{d_0}^2} - \frac{\pi}{3}ft \tag{4}$$

However, this solution produces imaginary numbers of the diameter for large time scales as it assumes that the frequency f of collisions leading to coalescence is independent of the drop size. Other considerations argue that the time evolution of size growth induced by coalescence is based on Brownian motion for nanoparticles and therefore scales with r to the power of 3.[29,30] For the merging of droplets the close proximity of droplets is required. Therefore, both the absolute concentration and the mobility of droplets is of importance. Coalescence is mostly imminent after initial flocculation or creaming and is complex due to its dependence on hydrodynamic and mechanical forces in combination with the behavior of all molecules present at the interface.[31] Ostwald ripening and coalescence are very hard to distinguish as both involve a growth in droplet size that can lead to heterogeneous distributions over long time periods in case of pure coalescence, while Ostwald ripening tends toward a homogeneous size.[32,33]

DOI: 10.1021/acs.langmuir.7b02852
Langmuir 2018, 34, 572−584

RESULTS

Kinetics of Phospholipid Adsorption. During the formation of an emulsion, the newly formed interface needs to be covered by the emulsifying surfactant as soon as the dispersed phase is divided into smaller droplets. To consider the influence and speed of the phospholipid (PL) diffusion on emulsion stability, changes in surface tension during drop formation were measured. Profile analysis tensiometry (PAT) was conducted to measure a three phase system with water in oil, containing a series of defined concentrations of DPPC. Figure 1 shows the change of interfacial tension $\gamma = \gamma(t)$ of a pendant water droplet in squalene with concentrations of 0.01, 0.05, and 0.5 mM DPPC in the bulk phase, respectively. Adsorption kinetics was studied over 2000 s; only for the highest concentration of DPPC pendant drops were unstable due to the low interfacial tension and detached from the capillary tip after 100−400 s. Figure 1 shows the characteristic time scales of adsorption kinetics which is governed by diffusion.[14,21] The interfacial tension at equilibrium γ_e can be assessed by extrapolating $\lim_{t\to\infty}\gamma(t)$ in a $t^{-1/2}$ versus $\gamma(t)$ plot.[14] To estimate the nonequilibrium state of DPPC adsorption at the squalene/water interface during the emulsification treatment of 10 min, the ratio $\gamma(10\text{ min})/\gamma_e$ was assessed.

The evolution of interfacial tension within the first 10 min after formation of a new interface refers to two characteristic time scales:

(a) The empirical experience that sonication over 10 min is an optimum for the minimization of droplet size: shorter sonication periods provide larger drops; longer periods do not minimize better, but reduce the derived count rates.
(b) The physicochemical time scale for the transition from regime A to regime B, which is a specific property of DPPC as emulsifier as can be seen by comparing the data for POPC in the Supporting Information.

A quantitative assessment of the data presented in Figure 1 is shown in Table 1, which shows that the interfacial tensions

Table 1. DPPC Concentrations in Squalene Used for Tensiometry for Which the Adsorption Kinetics and Non-Equilibrium Is Quantified by the Ratio of Interfacial Tension $\gamma(10\text{ min})$ to the Equilibrium Tension γ_e

c [mM]	$\gamma(10\text{ min})$	γ_e	$\gamma(10\text{ min})/\gamma_e$
0.01	22.7	19.9	1.14
0.05	11.7	9.59	1.22
0.5	8.5	4.98	1.71

in nonequilibrium at t = 10 min deviate from their respective equilibria. The relative deviation from equilibrium correlates with increasing concentration. At concentrations strongly below CAC, as is the case for c = 0.01 mM, the transient interfacial tension $\gamma(10\text{ min})$ is about 14% higher than equilibrium. At a concentration of c = 0.05 mM, which is about half of the CAC = 0.103 mM, the interfacial tension $\gamma(10\text{ min})$ is 22% higher than at equilibrium, while at c = 0.5 mM, i.e., about 5-fold above CAC, the transient $\gamma(10\text{ min})$ is as much as 70% higher than equilibrium. Even though the concentration gradient becomes larger, it takes longer for these concentrations to converge γ toward the respective equilibrium γ_e. We interpret this fact to be the result of the increasing surface pressure of the phospholipids covering the interface. This surface pressure is opposed to the diffusive transport of phospholipids to the interface and their adsorption. The interfacial tensions in equilibrium γ_e can be extrapolated from the limit of infinite time in a plot of $t^{-1/2}$ as justified by Hildebrandt et al.,[21] where three independent measurements were averaged as described in the methods section.

In correspondence with the adsorption characteristics of DPPC at squalene/water interfaces, it was decided to test the stability of water in squalene emulsions stabilized with DPPC in three repetitive steps of mechanical emulsification applied to the identical sample. This treatment was chosen to allow the slowly diffusing phospholipid to adsorb at the interface. Control experiments in the absence of DPPC did not yield sufficient signal strength, due to the rapid phase separation. Pretests had shown that the sonication periods longer than 10 min did not improve the emulsion characteristics, therefore two further repetitions of a sonication treatment of 10 min were performed, and the sample was monitored in between for 180 min to study its stability or destabilization, as described in the Materials and Methods section.

Repeated Sonication of an Identical Sample and Monitoring of Destabilization. The emulsion's evolution in terms of droplet size, PDI, and derived count rate was analyzed for 180 min as shown in Figure 2. The first sonication of the sample is represented by black squares, the second treatment is shown in open circles, and the third treatment in open triangles. Figure 2 contains six diagrams in two columns and three rows: the left-hand column, diagrams a, c, and e, represent data achieved for the DPPC concentration of 0.04 mM, while the right-hand column, diagrams b, d, and f, show the results for 0.4 mM. The first of the three rows, Figure 2a,b, shows the evolution of the z-averaged sizes, the second row, Figure 2c,d, the respective evolution of the PDI, and the third row, Figure 2e,f, the evolution of the derived count rate (DCR). The most obvious effect in the evolution of size and count rate is that two regimes exist in time: a first phase (A) of approximately 10 min with a higher growth rate in size, fitted with a power-law regression shown as straight line in the double-logarithmic plots. This first phase is followed by a second phase (B) with a smaller growth rate of size, i.e., smaller exponent of the power law regression. In contrast, the magnitude of the power-law exponent of the derived count rate's regression is smaller in the first phase and enlarged in the second phase, i.e., the negative slope is shallower in the first phase and becomes steeper in the second. As can be seen in Figure 2e, the power law regression of the third sonication sample remains constant until about 250 min, but then drops with a higher decrease rate. This pronounced drop in derived count rate takes place at a very low derived count rate (≤100 kcps). To start with, the first two phases in time will be considered, which are termed regime A and regime B in the following. To estimate their precise transition threshold, the intersections of linear regressions of the z-averaged sizes in regimes A and B are determined and summarized in Table 2. Table 2 shows the respective extrapolated initial z-averaged sizes $\bar{d}$ (at t = 1), i.e., about 1 min after completion of ultrasound treatment, and the slope m of a linear regression in double logarithmic plotting according to the equation:

$$\log \bar{d}(t) = m\cdot\log(t) + \log \bar{d}(1) \quad \text{or} \quad \bar{d}(t) = \bar{d}(1)\cdot t^m \tag{5}$$

DOI: 10.1021/acs.langmuir.7b02852
Langmuir 2018, 34, 572−584

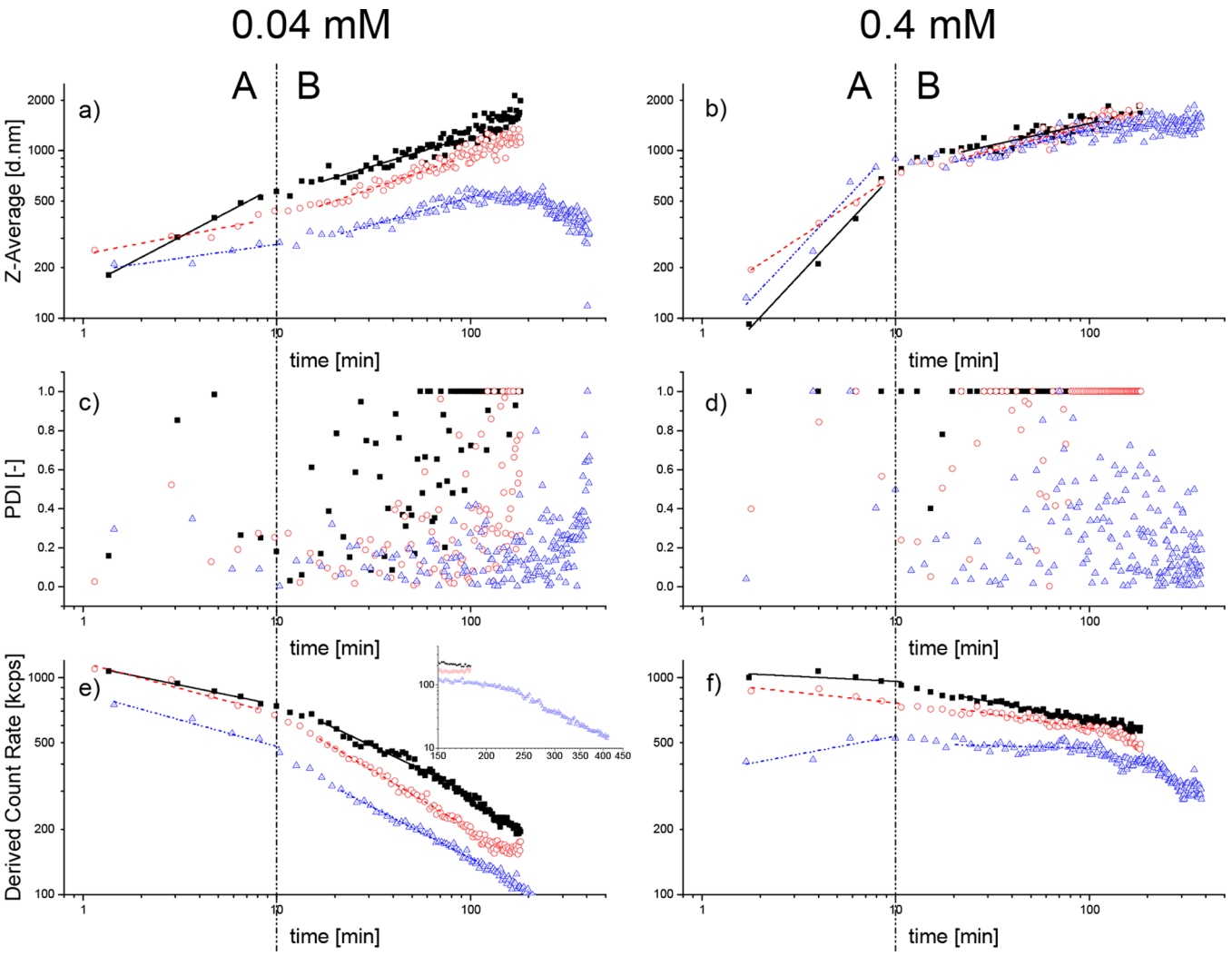

Figure 2. Evolution of emulsion stability after repeated sonication of an identical sample. The first, second, and third sonication is indicated by black squares, open circles, and open triangles, respectively. The two columns show DPPC concentrations of 0.04 mM and 0.4 mM, while the three rows depict the evolution of the *z*-averaged size, polydispersity index (PDI), and derived count rate (DCR), respectively. Destabilization of emulsions occurs in two regimes, termed A and B, distinguishable by a change of growth rate of size and decrease rate of DCR.

Table 2. Power-Law Regressions of the Size Evolution $\bar{D}(t)$ of W/O Nanoemulsions in Squalene/DPPC According to Eq 5 for the Data Shown in Figure 2

		extrapolated initial size $\bar{d}(1)$ [nm]		growth rate m $\left[\log\frac{nm}{min}\right]$ in eq 2		RMS error [nm] according to eq 3		
conc. [mM]	sonication	A	B	A	B	A	B	intersect A B [min]
0.04	first	151	242	0.60	0.34	5.64	12.05	6.25
	second	240	156	(0.21)	0.38	9.82	7.23	n.a.
	third	188	117	(0.16)	0.32	5.76	5.16	n.a.
0.4	first	42	443	1.24	0.25	19.86	17.21	10.8
	second	124	360	0.76	0.29	5.63	13.56	9.69
	third	63	379	1.22	0.27	30.43	13.98	6.52

which, in transferred to a linear plot, is identical to a power law regression with the exponent m.

Together with the root-mean-square error

$$\text{RMS Error} = \sqrt{\frac{1}{n}\sum_{i=1}^{n}(\bar{d}_{exp}(t_i) - \bar{d}(t_i))^2} \quad (6)$$

related to the power law regression. $\bar{d}_{exp}(t_i)$ is the measured z-averaged size at time t_i.

As can be seen graphically in Figure 2a,b, the distinction between regimes A and B in size evolution is only possible for the first sonication at c = 0.04 mM, while distinction is possible for all sonications at c = 0.4 mM. This distinction is reflected in Table 2 by the fact that the growth rates m are higher in regime A than in regime by regime B. The intersections of the power-law regressions of the size evolution of clearly distinguishable regimes A and B are in the range of 6.3 to 10.8 min, which confirms the visual observation of the transition taking place at

DOI: 10.1021/acs.langmuir.7b02852
Langmuir 2018, 34, 572−584

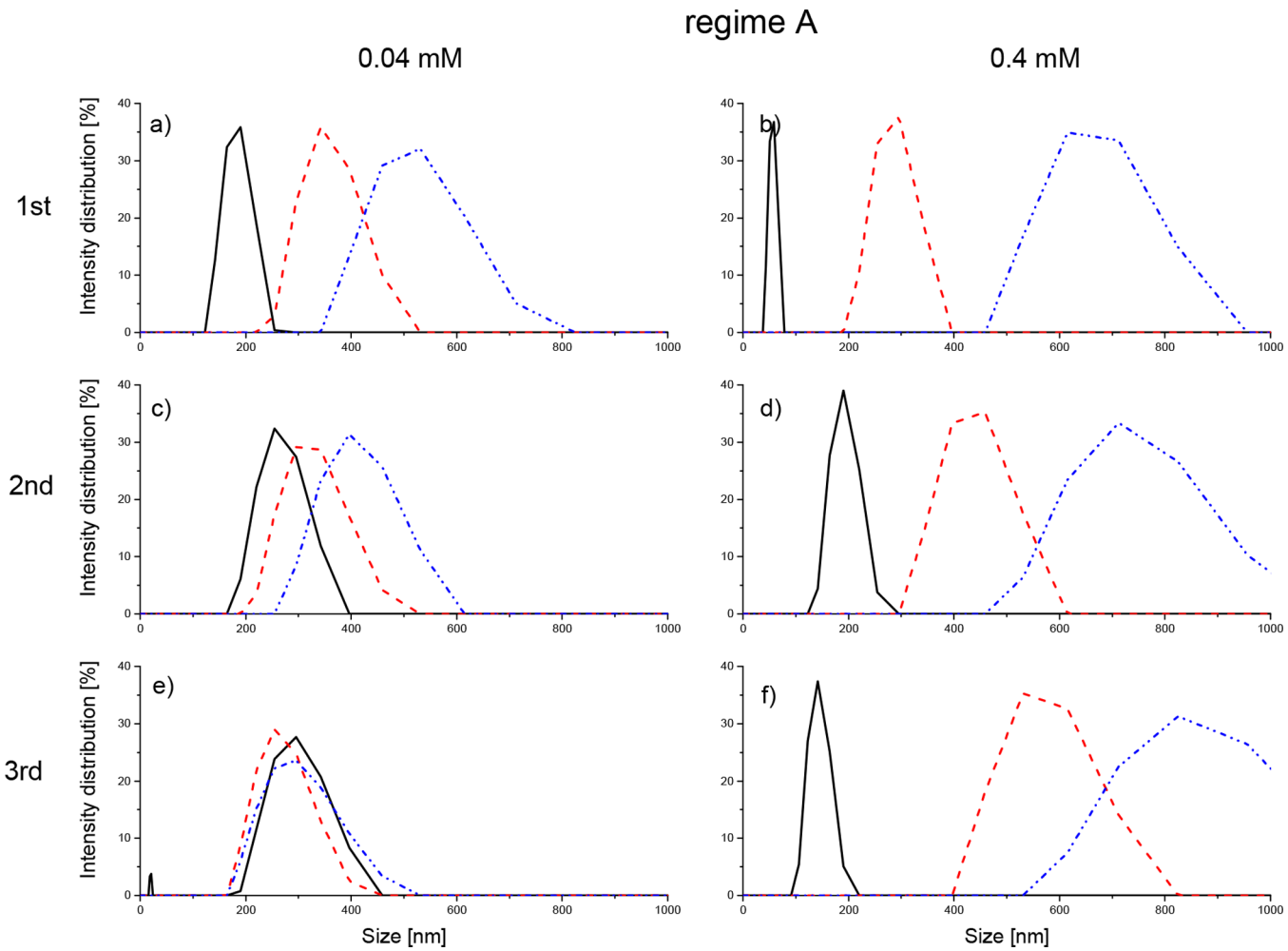

Figure 3. Evolution of the droplet size distributions in the W/O emulsion. The rows indicate the three sonications (1st, 2nd, and 3rd) applied on the same sample. The left column describes the development for a DPPC concentration c = 0.04 mM, while the right shows c = 0.4 mM. All distributions are recorded at discrete time points t during regime A (0−10 min), at $t \sim 1$ min (black line), $t \sim 5$ min (red dashed), and $t \sim 10$ min (blue dash-dot). Panel e of the 3rd sonication at 0.04 mM DPPC shows the most diminutive shift of the size distribution.

around 10 min. Intersections of the second and third sonication for c = 0.04 mM are not considered, as they do not show a clear change in growth and cannot be distinguished between the two regimes.

The nature of the two regimes and their transition will be explored by analyzing the growth rates m in dependence on c. In many former studies of nanoemulsion destabilization, Ostwald ripening was regarded as the main mechanism of droplet growth.[34] For Ostwald ripening, the averaged drop size grows according to $\bar{d}(t) \sim t^{1/3}$ (see eq 2). By contrast, for systems destabilized by coalescence, there is no commonly accepted theoretical approach to predict the increase in averaged drop size. Following the concept of Deminiere et al. 1999 (see eq 4), we could not find a satisfying linear relationship between time and $1/d^2$. It has to be taken into account that the emulsifying DPPC monolayer is in a very transient state in regime A (cf. Figure 1) since an increasing interfacial elasticity $\partial\Pi/\partial \ln A$ (with $\Pi = \gamma(0) - \gamma(t)$ being the film pressure) stabilizes against coalescence.[24] Due to the nonequilibrium conditions in regime A, we followed an empirical approach to interpret its size evolution. The growth rates m_A in regime A shown in Table 2 were $0.6 \leq m_A \leq 1.24$ for the first sonication at c = 0.04 mM and for all three sonications at c = 0.4 mM. Considering the mentioned settings, these results in regime A can be interpreted as a droplet destabilization mainly governed by coalescence. However, Ostwald ripening as well as a stabilization mechanism to be discussed below also influence the overall growth rate m_A, which therefore is a mixture of all mechanisms involved. The growth rates m_A for the second and third sonication of c = 0.04 mM are clearly smaller than 0.33, indicating the influence of a stabilizing effect that will be discussed in the next section.

In regime B, the growth rate m_B is between 0.32 and 0.38 for c = 0.04 mM, showing an almost exclusive influence of Ostwald ripening which scales with a theoretical growth rate $m_{Ostwald}$ = 0.33. For c = 0.4 mM, m_B is between 0.25 and 0.29, indicating hindered Ostwald ripening.

Comparing size evolution of the first, second, and third sonications graphically in Figure 2a,b, it becomes obvious that measured initial sizes $\bar{d}_{exp}$(1 min) are around 150 nm for c = 0.04 mM and around 100 nm for c = 0.4 mM with little differences between repetitions of sonications. Thus, repeated sonication does not change the initial averaged size which only depends on c. The influence of emulsifier concentration is obvious from Figure 1 since the interfacial tension is strongly decreased by the increase of c, leading to decreased resistance against the formation of new interfaces during sonication.

DOI: 10.1021/acs.langmuir.7b02852
Langmuir 2018, 34, 572−584

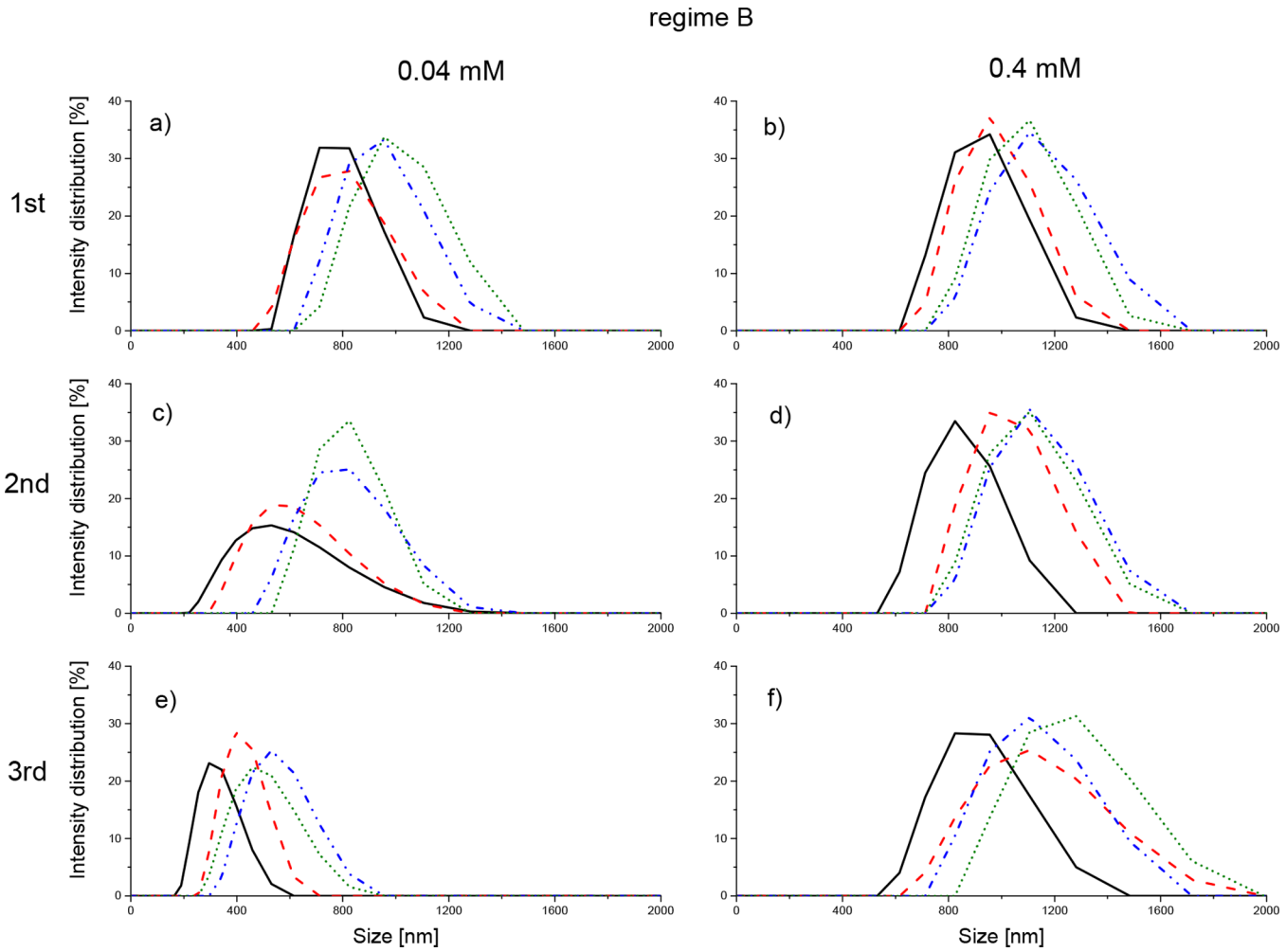

Figure 4. Evolution of the droplet size distributions in the W/O emulsion. The rows indicate the three sonications (1st, 2nd, and 3rd) applied on the same sample. The left column describes the development for a DPPC concentration c = 0.04 mM, while the right shows c = 0.4 mM. All distributions are recorded at discrete time points in regime B (15−90 min),), at $t \sim$ 15 min (black line); $t \sim$ 40 min (red dashed); $t \sim$ 70 min (blue dash-dot); and $t \sim$ 90 min (green dot).

Although repeated sonication does not decrease the initial averaged sizes, size evolution is clearly stabilized for the second and third sonication for c = 0.04 mM. While $\overline{d}(100\ \text{min}) > 1$ μm after the first sonication with $m_B \approx 0.34$, the maximum $\overline{d}$ is about 500 nm after the third sonication within an observation time of about 500 min and shrinking size, i.e. $m_B \leq 0$ after $t >$ 100 min.

For c = 0.4 mM the size evolution is very different from that at c = 0.04 mM. Overall, repeated sonication does not have a high influence on size evolution: In regime A repeated sonication even leads to slightly increased sizes, while in regime B the measured sizes are slightly smaller.

This means that repeated sonication clearly stabilizes the size evolution of nanoemulsions at concentrations c < CAC while it does not have a clearly visible effect on the size evolution for nanoemulsions at $c >$ CAC.

The evolution of the derived count rate (DCR) is in close correspondence to that of size: For c = 0.04 mM a kink is visible at the transitions between the two regimes with a stronger decrease rate in regime B than in regime A. The decrease in count rate is partially reversible in the sense that the identical sample has exactly the same count rate after the second sonication in regime A, while it is decreased by about 18% in regime B at 180 min. However, after the third sonication the DCR is decreases by about 38% in regime A and about 78% in regime B.

The time evolution of the DCR shows a much smaller decrease in time for c = 0.4 mM compared to 0.04 mM as can be seen from Figure 2f,e, respectively. In regime A, the decrease is minor after the first and second sonication (the DCR falls by about 10% within 10 min), while after the third sonication the DCR even increases by about 34% within 10 min. In regime B, the decrease rate is slightly higher, but the differences between the three sonications are much smaller: compared to the first sonication, the DCR decreases after the second sonication with equal decrease rate, but around 17% smaller magnitudes at 180 min. Even the longer-term decrease is much smaller for c = 0.4 mM compared to 0.04 mM. the final measured DCR magnitudes are around 300 kcps for the former, but only around 15 kcps for the latter.

The polydispersity of the two concentrations presented in Figure 2c,d shows a very diverse picture. After the first sonication, the PDI is initially at about 0.2 for c = 0.04 mM and rises to 1.0 after 180 min with a larger scatter of data in time, while the PDI is 1.0 for c = 0.4 mM at all times measured.

DOI: 10.1021/acs.langmuir.7b02852
Langmuir 2018, 34, 572−584

After the second sonication, the PDI is around 0.2 up to 30 min for c = 0.04 mM, but then starts to rise up to 1.0. For c = 0.4 mM the rise in PDI starts earlier and for $t \geq 100$ min the PDI is constantly 1.0.

However, the third sonication has a strong influence on the PDI at both concentrations. For c = 0.04 mM the PDI is on average 0.2 up to 300 min, but then rises to a PDI $\leq$ 1.0 for $t \leq$ 500 min. For c = 0.4 mM, the evolution of PDI is to a certain extent opposite: Initial PDI magnitude scatters over a large range, i.e., 0.1 < PDI < 1.0, while for t > 100 min the scatter is reduced to 0.1 < PDI < 0.6 and for t > 300 min it is even more reduced to 0.05 < PDI < 0.2.

In summary, the evolution of PDI shows that repeated sonications have a very positive effect in reducing the polydispersity both for DPPC concentrations below and above CAC. For c < CAC the reduction in polydispersity is visible after each sonication, while for c > CAC it is only visible for the third sonication.

As indicated by the evolution of the PDI, the droplet size distributions changed with time and with repeated sonication in a sample. Figure 3 shows the change in droplet size distribution in regime A, i.e., within a time frame of 1−10 min. Figure 3a depicts the first sonication with c = 0.04 mM and shows a narrow distribution at the start (∼1 min), with $\overline{d}$ = 180 nm and a half-maximum peak width w_{50} = 79 nm, which then develops to a larger size and wider distribution, up to $\overline{d}$(10 min) = 524 nm in size with a width of w_{50} = 246 nm. Obviously, the magnitude of mean size and PDI presented so far cannot sufficiently exhibit possible multimodal or very broad distributions. For this purpose, intensity-weighted size distributions from multiexponential fits were also evaluated in the following.

By contrast, the change in size and size distribution is not as strong during the second sonication (Figure 3c); the emulsion initially exhibits a slightly bigger size with $\overline{d}$ = 255 nm and a width of w_{50} = 118 nm, going up to a size of $\overline{d}$ = 414 nm and a width of w_{50}= 192 nm at ∼10 min. The third sonication follows the same pattern, showing only a slight increase in size and distribution, shown in Figure 3e. Here, the initial size of $\overline{d}$ = 211 nm increases only slightly, while the distribution width merely varies from w_{50} = 150 to 140 and 160 nm at ∼1, ∼5, and ∼10 min, respectively. Figure 3b,d,f for the first, second, and third sonication at c = 0.4 mM show a different pattern compared to the lower concentration c = 0.04 mM. Figure 3b also reveals a trend to larger sizes and distributions for the first sonication, with an initial size below $\overline{d}$ = 100 nm going up to 700 nm at ∼10 min and a widening of the distribution from w_{50} = 20 to 285 nm during the same interval. The second and third sonication, Figure 3d,f, show a growth in size and distribution width, increasing from a similar starting size at $\overline{d}$ = 200 nm to 700 and 900 nm with w_{50} = 400 nm at ∼10 min. Thus, the evolution on repeated sonication is completely opposite for c = 0.04 mM compared to c = 0.4 mM. For the former, both the size and width increase is diminished with every additional sonication.

Figure 4 describes the change in droplet size distributions for regime B, i.e., for time points above 10 min. Like Figure 3, two different concentrations with c = 0.04 mM and 0.4 mM are shown in two columns, while the rows display the three repetitive sonications of the same sample. In order to present the evolution of the distributions four discrete time points were chosen as representations for the regime at ∼15 min, ∼40 min, ∼70 min, and ∼90 min. Figure 4a shows the first sonication with c = 0.04 mM with a size growing from $\overline{d}$ = 814 to 1186 nm, while the distribution width stays almost constant with w_{50} = 182 to 217 nm and no fluctuation. The second sonication also shows a rise in size from $\overline{d}$ = 493 to 896 nm, though with smaller absolute numbers and interestingly a decrease in width from w_{50} = 271 nm going to 182 nm. This trend cannot be found in the third sonication, which again shows smaller sizes that grow over time, up to $\overline{d}$ = 458 nm, but an increase in width from w_{50} = 108 nm to167 nm. In comparison, the measurements with a concentration of c = 0.4 mM are more steady in size growth for all three sonications and a slight increase of size $\overline{d}$ from the first sonication to the second and third, but do not show a clear trend in distribution width. The width is varying between w_{50} = 197 to 246 nm for the first sonication, with similar values from w_{50} = 187 to 232 nm for the second sonication and slightly raised width w_{50} = 236 to 325 nm for the third sonication.

Overall, there is no clear trend for widening or sharpening of the distribution during regime B for c = 0.4 mM. In comparison to the evolution of the PDI as shown in Figure 2, Figure 4 shows that the monomodal peak distribution is not changed significantly by repeated sonications, while the total scatter of particle sizes (also comprising large particles not considered in the monomodal peak model) summarized by the PDI in fact decreases with repeated sonications.

The evolution of the distributions shown in Figures 3 and 4 are summarized by their respective values of $w_{50}(t)$ in Figure 5. The most obvious fact visible in Figure 5 is the sudden

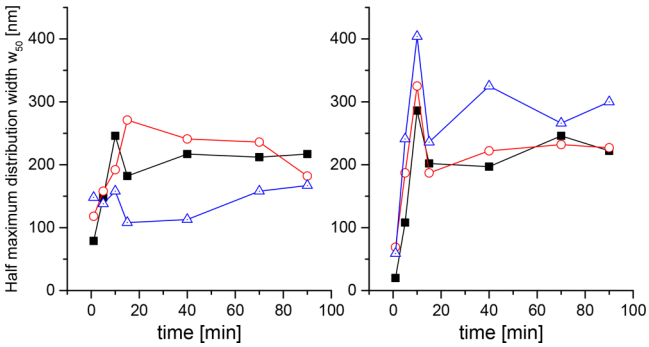

Figure 5. Evolution of the distribution width at half-maximum intensity $w_{50}(t)$. The first, second and third sonication is indicated by black squares, open circles, and open triangles, respectively. The left-hand side represents the concentration c = 0.04 mM DPPC, while the right-hand side shows c = 0.4 mM.

decrease of the half width w_{50} in the transition from regime A to regime B. This phenomenon will be interpreted in the following discussion section. Additional experiments with POPC were conducted and are presented in the Supporting Information.

DISCUSSION

All results presented in the previous section are summarized in a comprehensive morphological model, which interprets the effects by the formation of different structures and their interactions. Figure 6 shows models specified for the four states: the two regimes A and B and two phospholipid concentrations c < CAC and c > CAC, respectively.

The fact that the size growth rates m are higher in regime A for both c < CAC (only for first sonication) and c > CAC (all sonications) compared to all growth rates in regime B is

DOI: 10.1021/acs.langmuir.7b02852
Langmuir 2018, 34, 572−584

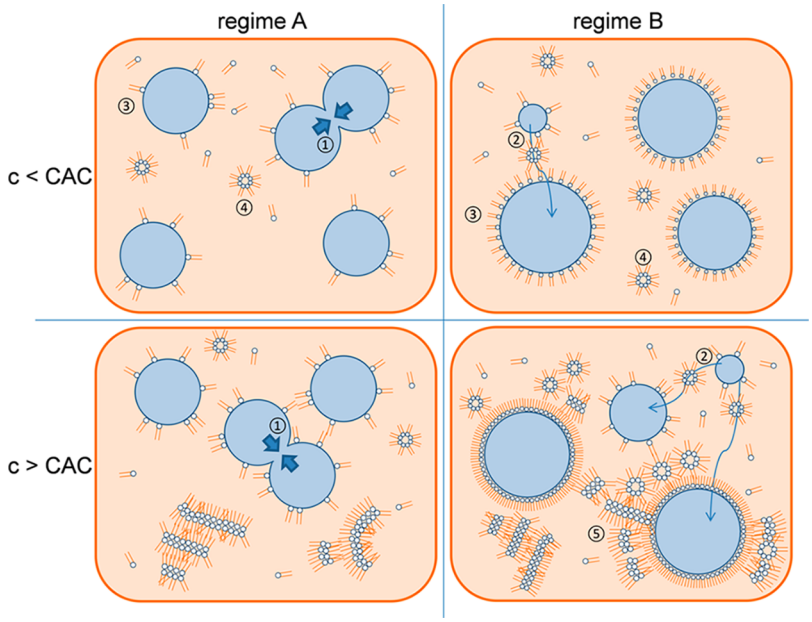

Figure 6. Interpretation of droplet growth by coalescence ① and Ostwald ripening ② in the two regimes A and B (columns) for 2 concentrations, below and above CAC (rows). The formation of pure DPPC monolayers ③ at the squalene/water interface and dispersed reverse micelles ④ is concluded to occur for c = 0.04 mM (below CAC) while for c = 0.4 mM (above CAC) the reverse micelles have been shown to attach to the monolayer[35] and also form bigger lipid aggregates[21]⑤.

interpreted to result from low initial interfacial densities of the emulsifying phospholipids. These low initial interfacial densities allow coalescence of drops colliding by Brownian motion in regime A, see detail ① in Figure 6. Droplet growth by coalescence leads to a compression of the interfacial densities due to the fusion of both monolayers (detail ③): For c < CAC the size increase within regime A is about 3-fold (only first sonication), while for c > CAC it is about 4−7-fold. The interfacial area per volume is compressed accordingly between 3-fold and 7-fold. As a result, coalescence is impeded increasingly due to the increasing surface pressure of the compressed lipid layer, which hinders further compression. Thus, the transition from regime A to B is interpreted to be the result of the suppression of coalescence by the advanced interfacial density of phospholipids and their steric repellence. As mentioned, for c < CAC an increased size growth rate m in regime A compared to regime B can only be found for the first sonication, while for the second and third sonication m is even slightly lower in regime A than in B (see Table 2).

This fact is interpreted as follows: the conformation of the drops in regime B at c < CAC allows the lipid layer to remain at the interface when the emulsion is sonicated for the second and third time. We assume that the conformation of the phospholipid for c < CAC in regime B is a monolayer state which can be retained during the second and third sonication when the sample is transformed back into regime A. In contrast, for c > CAC in regime B, we assume that the high lipid density leads to the association of reverse micelles[35] (④) and lipid aggregates at the phase boundary. The formation of lipid aggregates and their size is studied by Hildebrandt et al.[21] Upon the second and third sonication, the monolayers with associated reverse micelles are transformed into solid lipid aggregates which do not hinder coalescence once the sample is brought back into regime A. Accordingly, the size growth for c > CAC takes place for second and the third sonication in the same way as for the first sonication. In summary, it can be concluded that regime A is dominated by coalescence while regime B is dominated by Ostwald ripening (detail ②) as it was already discussed in the results section with respect to the exponents corresponding to the growth rates of the double logarithmic plots.

The morphological model visualized in Figure 6 is consistent not only for the evolution of the z-averaged size $\overline{d}_{exp}(t)$, but also with that of the polydispersity index PDI(t), the derived count rate DCR(t), and the evolution of the distribution half width $w_{50}(t)$. To start with, the morphological model in Figure 6 is compared with the derived count rate DCR(t) shown in Figure 2. The two most prominent effects for the evolution of DCR(t) as shown in Figure 2e,f are (i) the power law regressions appearing as linear slopes of the decrease rates in the double logarithmic plots in Figure 2, and (ii) the kink at the transition from regime A to B. These power law regressions are the result of the fact that the rate dependence of particles disappearing due to coalescence and Ostwald ripening always refers to the instantaneous number of existing particles, not on the initial number of particles, since the latter would form a linear regression in a linear plot. For c < CAC, the slopes of the DCR in regime A are all equal for the three sonications, while the size growth rates differ between the first sonication on the one hand and the second and third sonication on the other hand. Therefore, it is concluded that the evolution of the DCR in regime A does not depend on the size evolution. Instead, there is evidence that the decrease in DCR in regime A merely reflects the gradual diffusion of water from the smallest drops (with highest internal pressure) and adsorb to the hydrophilic moieties of DPPC molecules, which are self-organized as reversed micelles. The reverse micelles are regarded as the necessary vehicle of Ostwald ripening for the transfer of water molecules to other bulk water droplets. The formation of reverse micelles from phospholipids in a variety of organic phases was proved by recent publications[36,37] − their molar ratio of water to phospholipids w_0 is shown to be in the range

DOI: 10.1021/acs.langmuir.7b02852
Langmuir 2018, 34, 572−584

w_0 = 1−16 and their hydrodynamic diameter d_h is shown to depend on w_0 (d_h = 32.6 Å + 2.8 Å × w_0).[36] We conclude that DPPC reverse micelles are involved in Ostwald ripening, since water is practically insoluble in pure squalene. For c = 0.04 mM the molar ratio of water: DPPC is about 1100:1. This means that DPPC reverse micelles form a reservoir which can be filled with adsorbed water. Water bound to the DPPC reversed micelles no longer contributes to the DCR because of the small size of $d_h \leq 5$ nm so that the decrease of the DCR reflects the diffusive transfer of water from the bulk state to the reverse micelles. Would this water fraction have already reached other water droplets and contributed to their size growth, it would again add to the DCR and would not lead to a loss of signal, as it is the case. This interpretation of the "loss" of water to reverse micelles and ultimately to the cuvette walls and bottom is supported by the fact that after the second sonication the initial DCR is identical to the initial DCR after the first sonication. Thus, the decrease in the number of water droplets as indicated by the decreasing DCR is proved to be reversible.

A phenomenon to be interpreted is the steeper slope in the decrease of the DCR in regime B compared to regime A. This is interpreted as being caused by the consequences of Ostwald ripening which leads to the shrinking of droplets and at the same time causes a condensation of the emulsifying monolayers to their maximum. Further shrinking leads to a partial dissolution of DPPC from monolayer state, which then form reverse micelles dispersed in squalene, thus increasing the reservoir to which water can adsorb. This effect is further intensified for t > 200 min when the decrease rate of the DCR becomes even steeper. The latter is interpreted by an increasing number of drops that disappear completely, as is indicated by a decrease of the z-averaged size. Accordingly, the disappearance of droplets produces the dissolution of a higher amount of initial DPPC monolayers being transformed into reverse micelles as a reservoir that binds water and leads to a stronger decrease of the DCR.

Another property of the evolution of the DCR(t) to be interpreted is the difference in the decrease rates comparing c < CAC with c > CAC. Obviously, the DCR decreases much faster for c < CAC, both in regime A and in regime B. These differences between both concentrations in each regime are categorized as two independent facts and will be interpreted based on the morphological model shown in Figure 6. In regime A, the difference in decrease rate of the DCR is interpreted to be caused by much faster monolayer formation (cf. Figure 1), and, as a consequence, the association of the reverse micelles to the dense droplet monolayers as described by Campana et al. 2012.[35] Reverse micelles associated with droplets contribute to the light scattering signal intensity as they enlarge the droplet size while freely dispersed reverse micelles do not since they are too small compared to the drop population. In regime B, the different effect on the DCR of the two concentrations is interpreted to be caused by a thicker lipid layer around the droplets (detail ⑤), which reduces diffusion through the interface. Additionally, the diffusion of water to the reverse micelles associated with the lipid layer also contributes to the lower decrease rate of the DCR.

Looking at the evolution of the PDI(t) it can be seen that in general the PDI increases in time and decreases with increasing number of sonications for the same time point t. These findings are consistent with the fact that an increasing duration of sonication produces more homogeneous distributions, while both coalescence and Ostwald ripening globally produce more inhomogeneous droplet size distributions. A more detailed description of the effect of the instability mechanisms on the size distribution will be discussed for the interpretation of the evolution of $w_{50}(t)$. For the PDI(t), only the third sonication for c > CAC is focused since it is remarkable that the PDI remains low even for larger times, i.e., t > 100 min. The analogue sample for c < CAC shows the opposite for t > 100 min. The difference between the two samples is that for c < CAC the z-averaged size is always <500 nm, shrinking in average size with a steep decrease rate in the DCR and a DCR < 150 kcps. By contrast, for c > CAC the size is well above 1000 nm and the DCR is between 500 and 300 kcps. This means that for c < CAC, the droplets almost complete disappear by diffusion of water molecules to reverse micelles and ultimately the cuvette walls. By contrast, for c > CAC Ostwald ripening eliminates the fraction of small droplets with the remaining droplets showing a smaller polydispersity.

The evolution of the size distribution half width $w_{50}(t)$ is also in good agreement with the morphological model shown in Figure 6. The three most prominent properties shown for $w_{50}(t)$ in Figure 5 are (i) the steep increase in w_{50} during regime A with increases up to 1430% within 10 min.; (ii) the sudden and steep decrease of w_{50} around the transition from regime A to regime B with reductions of w_{50} of maximally 42% within 5 min.; (iii) the almost constant magnitude of $w_{50}(t)$ throughout regime B. A comparison of these attributes of $w_{50}(t)$ to the morphological model leads to the conclusion that during droplet growth dominated by coalescence in regime A $w_{50}(t)$ increases strongly, followed by a sharp decrease in w_{50} upon termination of coalescence due to stabilization by dense DPPC monolayers.[38] In regime B $w_{50}(t)$ is almost constant and grows only very slowly. All these conclusions can be justified by the factual properties of the two instability mechanisms: coalescence is a nonselective instability mechanism, particles of all sizes coalesce randomly by collision. It therefore leads to a strong increase of polydispersity since collisions create larger droplets, but small droplets prevail as long as they do not coalesce. In contrast, Ostwald-ripening is a selective instability mechanism since smaller particles disappear in high number with little size increase of the biggest particles. This explains the dramatic decrease in w_{50} upon the transition from regime A to regime B. The first w_{50} data in regime B are in the most extreme cases only 58% of the last w_{50} data in regime A. On average, the first w_{50} data in regime B drop to 78% of the last w_{50} data in regime A. In the long run, a sample developing under the exclusive influence of Ostwald ripening keeps its $w_{50}(t)$ practically constant, which means that the relative half maximal distribution width $w_{50}(t)/\overline{d}(t)$ decreases. In the size evolutions shown here, Ostwald ripening does not seem to be the exclusive instability mechanism. But still, a decrease of the relative width $w_{50}(t)/\overline{d}(t)$ occurs for 75% of all measured data in regime B while it only occurs for 17% of all measured data in regime A. In addition, an absolute decrease ($w_{50}(t_i) - w_{50}(t_{i-1})$ < 0) occurs in 47% of all recorded data in regime B. These numbers provide evidence that Ostwald ripening is the dominating, but not exclusive process of size evolution in regime B.

The calculated Ostwald ripening rates can be compared to literature results to verify the plausibility. Taylor exemplarily calculated the solubilities of alkanes in a continuous water phase by the application of LSW theory.[39] Figure 7 shows the Ostwald ripening rate in dependence of the molar volume of the dispersed phase, supplemented with values from

DOI: 10.1021/acs.langmuir.7b02852
Langmuir 2018, 34, 572−584

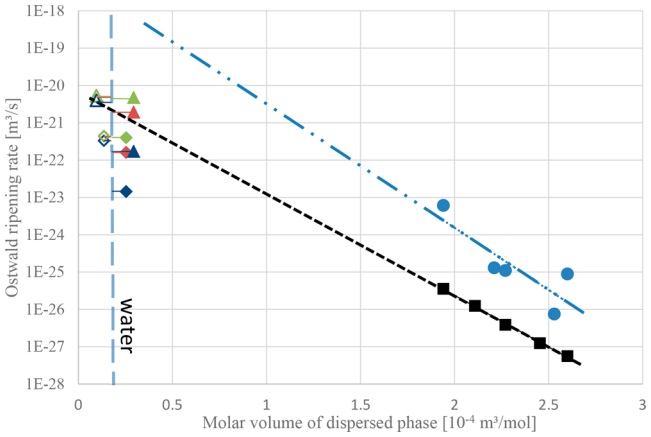

Figure 7. Ostwald ripening rates of different alkanes in water emulsions from Suriyarak et al.[40] (●) and Taylor[39] (■) compared to the Ostwald ripening rates for water in squalene emulsions for a concentration of 0.04 mM DPPC, for the 1st (blue diamond), 2nd (red), and 3rd (green) sonication. The calculated ripening rates are corrected (blue triangle, red, and green for the 1st, 2nd, and 3rd sonication, respectively) for the different viscosities of the continuous phases. All empty symbols represent the concentration of 0.4 mM DPPC accordingly. To improve the distinction of the different data points for water, some symbols are displayed at shifted V_m, but belong to water, indicated by the vertical dashed line.

Suriyarak[40] and Taylor[39] for the ripening rates of different alkanes in O/W emulsions with Tween and SDS as emulsifiers, respectively. Figure 7 shows that the measured values for W/O nanoemulsions emulsified by phospholipids are in the typical range for Ostwald ripening, considering that absolute numbers are much larger due to the smaller molar volume of water which accounts for much faster diffusive motion. An additional effect regarding the comparison of W/O nanoemulsions with O/W emulsion is the higher viscosity which was taken into account by applying a viscosity correction displayed in Figure 7 using different symbols. The remaining deviations of the Ostwald ripening rates from the literature and between different authors can be explained by the use of different surfactants and bulk fluids.

An analysis of the different effects on the Ostwald ripening rates for DPPC at 0.04 mM leads to the following results:

(a) The Ostwald ripening rate strongly decreases with increasing number of sonication cycle with the third sonication causing a reduction by a factor of 27.7 compared to the first cycle.
(b) When the viscosity difference of the continuous phase (squalene in our case, water in case of the cited data from literature) is to be compensated, a correction factor of 12.0 has to be applied.

For 0.4 mM DPPC the Ostwald ripening rate does not depend on the number of sonication cycles with the rate after the third sonication being only decreased by a factor of 1.3 compared to the rate after the first cycle. Thus, the morphological structure of the emulsifier around the water droplets does not change much for DPPC concentrations above CAC with increasing number of sonication cycles. By contrast, for c < CAC the tightness of the emulsifying layer increases strongly with every sonication cycle.

In the case of the shown literature, Tween and SDS are water-soluble emulsifiers which might be able to enhance the solubility of the alkanes and alkenes in water for the O/W emulsions, while in the case of W/O emulsions with squalene the emulsifier DPPC is more soluble in the oil and also strongly supports the diffusion of water in the continuous phase via reverse micelles as discussed for Figure 6. In an earlier publication Taylor discusses the impact of emulsifier concentration on the ripening rate, stating that below CAC the ripening rate is linear with the concentration, while above CAC no change is imminent.[41] The data published was conducted for O/W emulsions of alkanes, mostly with SDS as emulsifier. This is also in line with the presented model that accounts not only for the concentration, but the intermolecular arrangement of the emulsifier in terms of micelles and solubility.

Hoffmann et al. interpret small angle neutron scattering data on the exchange in nanoemulsions and conclude that only Ostwald ripening is the main mechanism for exchange.[42] They attribute the main factor for diffusion to the solubility of the dispersed alkene in water, hardly influenced by the choice of a specific surfactant. The observation of reduced Ostwald ripening with longer alkenes is in line with Kabalnov[32] and confirms theoretical expectations. The study does not vary the ratio of surfactant to dispersed phase fraction, like the presented study here, nor does it provide information on the kinetics of the surfactant. Hoffmann et al. also conclude that the coverage of the interface by an emulsifier will have an effect on diffusing molecules, as is suggested by our findings. The influence of the type and concentration of surfactant on Ostwald ripening is clearly shown by Weiss[43] and a connection is made between the surfactants' molecular state in dependence of the organic phase. The role of micelles during the transport is suggested, but not explored in more detail. Multilayer formation of DPPC was also investigated to stabilize other OW emulsion, with the conclusion to further investigate the role of micelles and liposomes in these emulsions[44,45]

■ CONCLUSION

It is well-known that W/O emulsions with phospholipids are very difficult to stabilize and show strong instabilities at higher rates of dispersed phase unless stabilized with other additives or thickeners,[46−48] but are stable for minutes to hours for dilute dispersed phases. The results shown here allow several conclusions concerning the governing principles of instability and novel practical applications of phospholipids for the stabilization of W/O emulsions. When a phospholipid is dissolved in the organic phase prior to emulsification its solubility and conformation in the organic phase strongly influences the structures to be formed. Due to the slow adsorption kinetics of phospholipids to cover the interfaces, three repetitions of a sonication treatment for mechanical dispersion of water in the organic phase were performed. These repetitive treatments disclosed a number of properties in the evolution of the averaged size, polydispersity, derived count rate, and size distribution half width of the sample. Evidence is provided that for the emulsifier DPPC an initial period of approximately 10 min the emulsion is strongly dominated by coalescence, followed by an abrupt decrease of the distribution width characterizing the persistent dominance of Ostwald ripening. This second period with the hydration of reverse micelles of phospholipids by diffusing water decides about the long-term properties of the emulsion.

For recent applications of W/O emulsions stabilized by phospholipids in the field of digital microfluidics or to produce liposomes from nanoemulsions, minimized sizes might be desirable. These can be achieved only for concentrations c <

DOI: 10.1021/acs.langmuir.7b02852
Langmuir 2018, 34, 572−584

CAC with repeated sonication leading to an intermediate stabilization of the emulsion droplets <500 nm after the third sonication cycle. These droplets are covered by monomolecular phospholipid layers and exhibit low polydispersity. However, the properties of reverse micelles of phospholipids in adsorbing water rapidly decrease the number of dispersed droplets which can go down to complete dissolution after a few hours. If droplet sizes >1 μm are acceptable for the purpose of the application, c > CAC is more promising for the achievement of W/O emulsions with longer stability characteristics. For such W/O emulsions, which are stabilized by dense monolayers,[49,50] associated reverse micelles and lipid aggregates, repeated mechanical treatment by, e.g., sonication proves to be beneficial to reduce the polydispersity and shows much slower diffusion from the water droplets to the reverse micelles compared to W/O emulsion with lower phospholipid concentrations.

DPPC is proved to be a much more suitable candidate for the emulsification of nanoemulsions than POPC. DPPC allows one to examine the periods of destabilization and interaction with the continuous organic phase much better, also leading to a consistent interpretation on the instability mechanism. The results gained for POPC are in line with the morphological hypothesis for DPPC, thus contributing toward the understanding of nanoemulsion stability.

■ ASSOCIATED CONTENT

Supporting Information

The Supporting Information is available free of charge on the ACS Publications website at DOI: 10.1021/acs.langmuir.7b02852.

Details of the experiments with POPC (PDF)

■ AUTHOR INFORMATION

ORCID

Robbert Jan Kok: 0000-0003-4933-3968

Gero Leneweit: 0000-0002-3783-1217

Notes

The authors declare no competing financial interest.

■ ACKNOWLEDGMENTS

We gratefully acknowledge assistance in sample preparations and measurements by Maryam Aalami and technical support by Stefan Nikolaus. The research leading to these results has received funding from the People Programme (Marie Curie Actions) of the European Union's Seventh Framework Programme FP7/2007−2013/under REA Grant Agreement No. 324275 (project acronym: decent AID) and from the Phospholipid Research Center (Heidelberg, Germany). Phospholipids were donated by Lipoid GmbH (Ludwigshafen, Germany).

■ REFERENCES

(1) McClements, D. J.; Gumus, C. E. Natural emulsifiers - Biosurfactants, phospholipids, biopolymers, and colloidal particles: Molecular and physicochemical basis of functional performance. *Adv. Colloid Interface Sci.* **2016**, *234*, 3−26.

(2) van Hoogevest, P.; Wendel, A. The use of natural and synthetic phospholipids as pharmaceutical excipients. *Eur. J. Lipid Sci. Technol.* **2014**, *116*, 1088−1107.

(3) Wu, Y.; Wang, T. Soybean lecithin fractionation and functionality. *J. Am. Oil Chem. Soc.* **2003**, *80*, 319−326.

(4) Kabalnov, A.; Tarara, T.; Arlauskas, R.; Weers, J. Phospholipids as Emulsion Stabilizers: 2. Phase Behavior versus Emulsion Stability. *J. Colloid Interface Sci.* **1996**, *184*, 227−235.

(5) Ushikubo, F. Y.; Cunha, R. L. Stability mechanisms of liquid water-in-oil emulsions. *Food Hydrocolloids* **2014**, *34*, 145−153.

(6) Friberg, S., Ed. *Food Emulsions*, 4th ed.; Dekker: New York, 2004.

(7) Kabalnov, A.; Weers, J.; Arlauskas, R.; Tarara, T. Phospholipids as Emulsion Stabilizers. 1. Interfacial Tensions. *Langmuir* **1995**, *11*, 2966−2974.

(8) Delmas, T.; Piraux; Couffin, A.-C.; Texier, I.; Vinet, F.; Poulin, P.; Cates, M. E.; Bibette, J. How To Prepare and Stabilize Very Small Nanoemulsions. *Langmuir* **2011**, *27*, 1683−1692.

(9) Freitas, S.; Hielscher, G.; Merkle, H. P.; Gander, B. Continuous contact- and contamination-free ultrasonic emulsification-a useful tool for pharmaceutical development and production. *Ultrason. Sonochem.* **2006**, *13*, 76−85.

(10) Behrend, O.; Schubert, H. Influence of hydrostatic pressure and gas content on continuous ultrasound emulsification. *Ultrason. Sonochem.* **2001**, *8*, 271−276.

(11) Picart, L.; Thiebaud, M.; René, M.; Pierre Guiraud, J.; Cheftel, J. C.; Dumay, E. Effects of high pressure homogenisation of raw bovine milk on alkaline phosphatase and microbial inactivation. A comparison with continuous short-time thermal treatments. *J. Dairy Res.* **2006**, *73*, 454−463.

(12) Kleinig, A. R.; Middelberg, A. P.J. On the mechanism of microbial cell disruption in high-pressure homogenisation. *Chem. Eng. Sci.* **1998**, *53*, 891−898.

(13) He, Q.; Zhang, Y.; Lu, G.; Miller, R.; Möhwald, H.; Li, J. Dynamic adsorption and characterization of phospholipid and mixed phospholipid/protein layers at liquid/liquid interfaces. *Adv. Colloid Interface Sci.* **2008**, *140*, 67−76.

(14) Li, J.; Miller, R.; Möhwald, H. Characterisation of phospholipid layers at liquid interfaces. 1. Dynamics of adsorption of phospholipids at the chloroform/water interface. *Colloids Surf., A* **1996**, *114*, 113−121.

(15) Li, J.; Miller, R.; Wüstneck, R.; Möhwald, H.; Neumann, W. A. Use of pendent drop technique as a film balance at liquid/liquid interfaces. *Colloids Surf., A* **1995**, *96*, 295−299.

(16) Ishii, F.; Nii, T. Properties of various phospholipid mixtures as emulsifiers or dispersing agents in nanoparticle drug carrier preparations. *Colloids Surf., B* **2005**, *41*, 257−262.

(17) Fox, C. B. Squalene Emulsions for Parenteral Vaccine and Drug Delivery. *Molecules* **2009**, *14*, 3286−3312.

(18) Pautot, S.; Frisken, B. J.; Weitz, D. A. Production of Unilamellar Vesicles Using an Inverted Emulsion. *Langmuir* **2003**, *19*, 2870−2879.

(19) Hu, P. C.; Li, S.; Malmstadt, N. Microfluidic Fabrication of Asymmetric Giant Lipid Vesicles. *ACS Appl. Mater. Interfaces* **2011**, *3*, 1434−1440.

(20) Elani, Y.; de Mello, A. J.; Niu, X.; Ces, O. Novel technologies for the formation of 2-D and 3-D droplet interface bilayer networks. *Lab Chip* **2012**, *12*, 3514−3520.

(21) Hildebrandt, E.; Sommerling, J.-H.; Guthausen, G.; Zick, K.; Stürmer, J.; Nirschl, H.; Leneweit, G. Phospholipid adsorption at oil in water versus water in oil interfaces: Implications for interfacial densities and bulk solubilities. Colloids and Surfaces A. *Colloids Surf., A* **2016**, *505*, 56−63.

(22) Hildebrandt, E.; Dessy, A.; Sommerling, J.-H.; Guthausen, G.; Nirschl, H.; Leneweit, G. Interactions between Phospholipids and Organic Phases: Insights in Lipoproteins and Nanoemulsions. *Langmuir* **2016**, *32*, 5821−5829.

(23) Westesen, K.; Wehler, T. Investigation of the Particle Size Distribution of a Model Intravenous Emulsion. *J. Pharm. Sci.* **1993**, *82*, 1237−1244.

(24) Tadros, T. Application of rheology for assessment and prediction of the long-term physical stability of emulsions. *Adv. Colloid Interface Sci.* **2004**, *108−109*, 227−258.

DOI: 10.1021/acs.langmuir.7b02852
Langmuir 2018, 34, 572−584

(25) Lifshitz, I. M.; Slyozov, V. V. Kinetics of Diffusive Decomposition of Supersaturated Solid Solutions. *J. Exp. Theor. Phys.* **1959**, *8*, 331−339.
(26) Higuchi, W. I.; Misra, J. Physical Degradation of Emulsions Via the Molecular Diffusion Route and the Possible Prevention Thereof. *J. Pharm. Sci.* **1962**, *51*, 459−466.
(27) Koroleva, M. Y.; Yurtov, E. V. Effect of Ionic Strength of Dispersed Phase on Ostwald Effect of Ionic Strength of Dispersed Phase on Ostwald Ripening in Water-in-Oil Emulsions. *Colloid J.* **2003**, *65*, 40−43.
(28) Deminiere, B.; Stora, T.; Colin, A.; Leal-Calderon, F.; Bibette, J. Surfactant Phase Transition Inducing Coalescence in Dense Emulsions. *Langmuir* **1999**, *15*, 2246−2249.
(29) Wang, H.; Davis, R. H. Droplet Growth Due to Brownian, Gravitational, or Thermocapillary Motion and Coalescence in Dilute Dispersions. *J. Colloid Interface Sci.* **1993**, *159*, 108−118.
(30) Hansen, T. W.; Delariva, A. T.; Challa, S. R.; Datye, A. K. Sintering of catalytic nanoparticles: Particle migration or Ostwald ripening? *Acc. Chem. Res.* **2013**, *46*, 1720−1730.
(31) McClements, D. J. Critical review of techniques and methodologies for characterization of emulsion stability. *Crit. Rev. Food Sci. Nutr.* **2007**, *47*, 611−649.
(32) Kabalnov, A. Ostwald Ripening and Related Phenomena. *J. Dispersion Sci. Technol.* **2001**, *22*, 1−12.
(33) Piorkowski, D. T.; McClements, D. J. Beverage emulsions: Recent developments in formulation, production, and applications. *Food Hydrocolloids* **2014**, *42*, 5−41.
(34) Wooster, T. J.; Golding, M.; Sanguansri, P. Impact of Oil Type on Nanoemulsion Formation and Ostwald Ripening Stability. *Langmuir* **2008**, *24*, 12758−12765.
(35) Campana, M.; Webster, J. R. P.; Lawrence, M. J.; Zarbakhsh, A. Structural conformation of lipids at the oil-water interface. *Soft Matter* **2012**, *8*, 8904−8910.
(36) Abel, S.; Galamba, N.; Karakas, E.; Marchi, M.; Thompson, W. H.; Laage, D. On the Structural and Dynamical Properties of DOPC Reverse Micelles. *Langmuir* **2016**, *32*, 10610−10620.
(37) Kittipongpittaya, K.; Panya, A.; McClements, D. J.; Decker, E. A. Impact of Free Fatty Acids and Phospholipids on Reverse Micelles Formation and Lipid Oxidation in Bulk Oil. *J. Am. Oil Chem. Soc.* **2014**, *91*, 453−462.
(38) Rodriguez Patino, J.; Caro, A.; Rodriguez Nino, M.; Mackie, A.; Gunning, A.; Morris, V. Some implications of nanoscience in food dispersion formulations containing phospholipids as emulsifiers. *Food Chem.* **2007**, *102*, 532−541.
(39) Taylor, P. Ostwald ripening in emulsions: estimation of solution thermodynamics of the disperse phase. *Adv. Colloid Interface Sci.* **2003**, *106*, 261−285.
(40) Suriyarak, S.; Weiss, J. Cutoff Ostwald ripening stability of alkane-in-water emulsion loaded with eugenol. *Colloids Surf., A* **2014**, *446*, 71−79.
(41) Taylor, P. Ostwald ripening in emulsions. *Adv. Colloid Interface Sci.* **1998**, *75*, 107−163.
(42) Hoffmann, I.; Simon, M.; Hörmann, A.; Gravert, T.; Heunemann, P.; Rogers, S. E.; Gradzielski, M. Kinetics of Oil Exchange in Nanoemulsions Prepared with the Phase Inversion Concentration Method. *Langmuir* **2016**, *32*, 12084−12090.
(43) Weiss, J.; Herrmann, N.; McClements, D. J. Ostwald Ripening of Hydrocarbon Emulsion Droplets in Surfactant Solutions. *Langmuir* **1999**, *15*, 6652−6657.
(44) Wiącek, A. E. Effect of ionic strength on electrokinetic properties of oil/water emulsions with dipalmitoylphosphatidylcholine. *Colloids Surf., A* **2007**, *302*, 141−149.
(45) Chaprenet, J.; Berton-Carabin, C. C.; Elias, R. J.; Coupland, J. N. Effect of interfacial properties on the reactivity of a lipophilic ingredient in multilayered emulsions. *Food Hydrocolloids* **2014**, *42*, 56−65.
(46) Knoth, A.; Scherze, I.; Muschiolik, G. Stability of water-in-oil-emulsions containing phosphatidylcholine-depleted lecithin. *Food Hydrocolloids* **2005**, *19*, 635−640.
(47) Weete, J. D.; Betageri, S.; Griffith, G. L. Improvement of lecithin as an emulsifier for water-in-oil emulsions by thermalization. *J. Am. Oil Chem. Soc.* **1994**, *71*, 731−737.
(48) Hasenhuettl, G. L.; Hartel, R. W. *Food Emulsifiers and Their Applications*, 2nd ed.; Springer: New York, 2008.
(49) Guzmán, E.; Liggieri, L.; Santini, E.; Ferrari, M.; Ravera, F. Effect of Hydrophilic and Hydrophobic Nanoparticles on the Surface Pressure Response of DPPC Monolayers. *J. Phys. Chem. C* **2011**, *115*, 21715−21722.
(50) Guzmán, E.; Orsi, D.; Cristofolini, L.; Liggieri, L.; Ravera, F. Two-dimensional DPPC based emulsion-like structures stabilized by silica nanoparticles. *Langmuir* **2014**, *30*, 11504−11512.

DOI: 10.1021/acs.langmuir.7b02852
Langmuir 2018, 34, 572−584